Journal of Thermal Analysis and Calorimetry (2020) 140:1597–1610
https://doi.org/10.1007/s10973-019-09148-x

Investigation on the effect of different coated absorber plates on the thermal efficiency of the flat-plate solar collector

Seyed Ali Sakhaei[1] · Mohammad Sadegh Valipour[1]

Received: 26 September 2019 / Accepted: 1 December 2019 / Published online: 14 December 2019

Abstract

The aim of the present work is to compare thermal efficiency of three flat-plate collectors, which are different in the type of coatings used in the absorber plate. The thermal efficiency of the collector was investigated using three types of absorber plate: the black painted, the black chrome coating, and the carbon coating. The thermal performance of the collectors was considered based on American Society of Heating, Refrigerating and Air-Conditioning Engineers Standard 93 (2010). The volume flow rate varied from 0.5 to 1.5 L min^{-1}. The field emission scanning electron microscope images demonstrated that the carbon coating had high absorption due to trapping the light and avoiding the reflection of the light. The collector with the carbon-coated absorber plate at the flow rate of 1.5 L min^{-1} has the maximum thermal efficiency of approximately 69.4%. Furthermore, the thermal efficiency of the carbon-coated absorber plate and black chrome-coated absorber plate is averagely 13% and 11.3% higher than the black-painted absorber plate, respectively. Additionally, the removed energy parameter ($F_R U_L$) at the flow rate of 1.5 L min^{-1} decreases approximately 35.4% for the collector with the carbon-coated absorber plate and 28.4% for the collector with the black chrome-coated absorber plate compared to the black-painted absorber plate.

Keywords Flat-plate collector · Coated absorber plate · Thermal efficiency · ASHRAE Standard · Removed energy parameter

List of symbols

A_c	Area of the absorber plate, (m^2)
D	Riser tube diameter, (m)
h	Heat transfer coefficient, (W $m^{-2}K^{-1}$)
Q_u	The useful energy gain, (W)
T_a	Ambient temperature, (K)
T_o	Outlet temperature, (K)
T_{in}	Inlet temperature, (K)
$T_{f,o}$	Outlet fluid temperature, (K)
$T_{f,i}$	Inlet fluid temperature, (K)
$T_{f,o,initial}$	Outlet initial fluid temperature, (K)
C_p	Specific heat, (J kg^{-1})
G	Solar radiation, (W m^{-2})
F_R	Heat removal factor
$\dot{m}$	Mass flow rate, (kg s^{-1})
U_L	Heat loss coefficient, (W m^{-2} K^{-1})

Subscripts and superscripts

a	Ambient
f	Fluid
e	Emissivity
i	Inlet
o	Outlet

Greek symbols

α	Plate absorptance
η	Thermal efficiency of collector
τ	Glass cover transmittance
δR	Uncertainty in the result, generic
δX_j	Uncertainty in the jth variable

Abbreviations

FPC	Flat-plate collector
Re	Reynolds number, $\rho U D_h / \mu_f$
PH	Power of hydrogen

✉ Mohammad Sadegh Valipour
msvalipour@semnan.ac.ir

Seyed Ali Sakhaei
ali.sakhaei@semnan.ac.ir

[1] Faculty of Mechanical Engineering, Semnan University, Semnan 19111-35131, Iran

Introduction

The growing demand for energy resources and the concern about increasing environmental pollution lead humans to seek and consider clean energies. Solar energy is a kind of

energy that has been highly considered owing to its accessibility and less environmental impacts. Flat-plate collectors (FPCs) are solar systems absorbing solar radiation and transferring it to working fluid. They are widely used in low-temperature applications such as water heating production and space heating [1]. In the last decade, several studies have been conducted in the field of improving heat transfer and thermal efficiency of FPCs The methods of thermal performance enhancement of FPCs can be categorized into two main groups: i) passive methods and ii) active methods [2]. In passive methods, no external forces have been used. So, it receives more attention [3, 4].

In passive methods, turbulators such as wire coils, disks, and twisted tapes have been used [5]. The heat transfer increases by using twisted tapes, because the use of twisted tapes causes the decrease in hydraulic diameter and increase in swirl generation [6]. In a parametric study to relate the fluid and flow characteristics with the heat transfer enhancement study done by Garcia et al. [7], wire coils have been used to enhance the heat transfer of a tube-on-sheet solar panel. The enhanced collector increases the thermal efficiency values by 4.5%. In another study, using twisted tapes with lengths of 100, 200, and 300 mm for twist ratios 3 and 5 was investigated by Jaisankar et al. [5]. The results show that Nusselt number and friction factor increased by 19% and 29%, respectively. In another study by Ananth et al. [6, 8], the overall instantaneous thermal efficiency improved between 53.3 and 38.7% when using twisted tape with rod and spacer in a thermosiphon solar water heating system compared with plain tube collector. The results present that the Nusselt number decreases by 11 and 19% for twist fitted with rod and twist with spacer, respectively. García et al. [7] have applied wire coil to enhance heat transfer in a typical flat-plate solar water heater. According to the results, average improvement in thermal efficiency from 14 to 31% in different cases has been obtained. Using nanofluids as the working fluid, Javaniyan Jouybari et al. [9] have investigated the effects of SiO_2/deionized water nanoparticles on the thermal performance of a flat-plate solar collector. Their results showed that the thermal efficiency was improved up to 8.1% with the presence of nanofluid.

Porous media can increase the thermal efficiency of FPCs due to increasing contact surface with flow [10]. Chen et al. [11] performed an experimental investigation on the effect of porous structure on the thermal efficiency of a FPC. An integrated aluminum foam porous structure filled with paraffin was used to enhance the heat transfer performance of a flat-plate solar collector. The results demonstrated that the using of the foam has significant effect on the heat transfer and melting rate of paraffin.

The use of nanofluids as working fluids is another passive method, which is used to increase the thermal efficiency of FPCs [12–14]. Nanofluids increase the thermal conductivity of fluids and, as a result, lead to the increase in heat transfer [15]. In a research done by Tayebi et al. [16], the effect of Al_2O_3 nanofluid and TiO_2 nanofluid was investigated on the thermal performance of a parabolic trough collector. The maximum efficiency was 34.51% for TiO_2 nanofluid. Another example of using TiO_2 nanofluid is the study by Said et al. [17]. According to the results, the energy efficiency is enhanced by 76.6% for 0.5 kg min^{-1} flow rate and 0.1% volume fraction. Noghrehabadi et al. [18] studied the conical shape of a solar water heater at different flow rates. The maximum value of thermal efficiency was approximately 60%.

A brief review on other studies shows that the use of turbulators, porous media, and nanofluids can help to improve the thermal performance of FPCs, but it can lead to using more materials and high pressure drop [19]. Therefore, researchers are studying other methods to improve heat transfer, which have lower costs and lower pressure drop. The use of selective coatings on the absorber plate can be another effective method to improve the thermal efficiency of FPCs [20–22]. The selective coatings have high absorptivity at short wavelengths and low emissivity at long wavelengths [23]. The thermal efficiency of the FPC can increase to 28% when the absorptivity increases from 0.8 to 0.98 [24]. The deposition of a four-layer composite film structure, W/AlSiOx:W(HA)/AlSiOx:W(LA)/AlSiOx, on stainless steel with the absorptivity of 94–95.5% was suitable for solar thermal applications [25]. The Mo/ZrSiN/ZrSiON/SiO_2 coating on stainless steel had the solar absorbance of 0.94 [26]. The absorptivity of the sputtered black chrome was between 0.92 and 0.96 [27]. The process of Cu/CuOx deposition on copper was performed by electrodeposition and spray pyrolysis deposition. The absorptivity varied from 0.87 to 0.95 [28]. The rough graphite–aluminum (C/Al_2O_3/Al) had the solar absorptance of 0.9 [29]. The effects of using epoxy coating (zinc phosphate) and an anti-corrosive with catalyst on the optical absorptivity were investigated to select the best one to use in flat-plate collectors as the coating of the absorber plate. The absorptivity of the epoxy coating was between 0.93 and 0.95 [30]. The effects of using nanofluid and selective absorber on the exergy efficiency and the thermal efficiency were examined. The effect of variation of the ratio of emissivity to absorptivity on the exergy efficiency was significant. The exergy efficiency and the thermal efficiency increased by 8% and 10.5% with an increase of 7.5% in optical efficiency [31]. The graphene was deposited on the copper oxide substrate as a selective coating. The use of graphene coating increased maximum efficiency from 39.5 to 69.4% compared to the reference collector [32]. Kasaeian et al. [33] measured the absorptance of black chrome, nickel chrome, and matt black paint, which was about 97.4%, 98%, and 91.4%. In another study, Kasaeian et al. [34] demonstrated that the thermal efficiency of a parabolic trough collector increased by about 10% by using black

chrome coating on the absorber tube in comparison with a black-painted absorber tube.

The literature review expresses the important effect of the coating on the absorptivity of material and a shortcoming in investigating the effects of selective coating absorber plates on the FPSCs' efficiency. For this purpose, in the present study, the impacts of using three types of absorber plate, namely the black painted, the black chrome coating, and the carbon coating, were investigated on the FPC thermal efficiency. It should be noted that these coatings were selected because of their high absorptivity at short wavelengths and low emissivity at long wavelengths which cause to enhancement of the collection of thermal energy [24–27, 32]. Furthermore, they are selected due to good optical properties, good thermal conductivity, and great accessibility. To the best of our knowledge, the effect of the black painted, the black chrome coating, and the carbon coating on the absorber plate of FPC has been rarely investigated. The performance of FPC was examined based on ASHRAE Standard 93 [35]. In addition, the thermal efficiency of FPCs with different coated absorber plates at various flow rates was compared. The absorbed and removed energy parameters were explained, and the impact of different coatings on the value of these parameters was presented. Since this study has not been conducted before, it is necessary to consider the effect of the black painted, the black chrome coating, and the carbon coating on the thermal efficiency of the flat-plate collector.

Experimental procedure

In this section, the specifications of the FPSC and the measurement tools that were used in the test are presented.

To conduct experimental tests, a FPSC was designed with an area of 0.5824 m^2. Figure 1 shows the experimental setup and the schematic diagram of it. The experiments were performed at Semnan University, Semnan, Iran (latitude 35°34′ N longitude 53°22′ E).

At first, for the construction of the FPSC setup, three copper absorber plates were coated with three selective coatings, i.e., the black painted, the black chrome, and the carbon coating. The four one-meter copper risers were welded on the back of each absorber plates, and then, the assembly of absorber plate and risers were connected to the top and bottom headers. After the galvanized collector frame was prepared, the casing including the set of absorber plate, risers, and headers were isolated by elastomer insulation with the thickness of 10 cm covering its three sides. Then, a glass cover was installed and slant angle was set in 45 degree. In this study, three assembly plates, risers, and headers were used. The difference between these assemblies is their coatings. After the preparation of the collector setup,

(a)

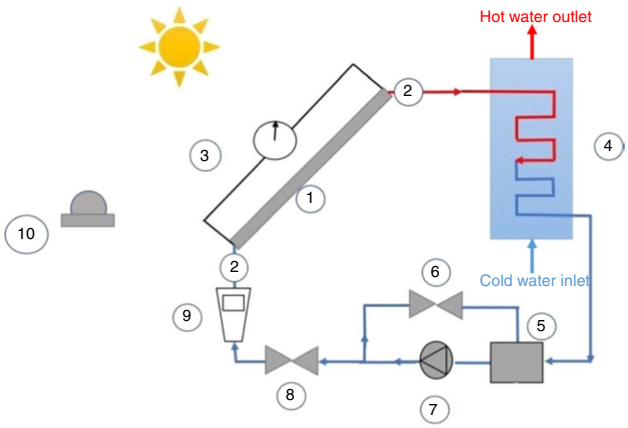

(b)

Fig. 1 **a** Experimental setup, **b** the schematic diagram of hydraulic cycle (1—flat-plate collector, 2—temperature sensor, PT100, 3—pressure transmitter, 4—heat exchanger, 5—reservoir tank, 6—valve, 7—pump, 8—valve, 9—flowmeter, 10—solar power meter, TES-1333R.)

two storage tanks were also constructed. In the first storage tank, helical copper tubes were devised, which contain the working fluid that is reaching the ambient temperature by water in the tank (Fig. 1b). The second storage tank is for saving and storing water. According to Fig. 1b, the working fluid enters the helical copper tubes, which are within the first storage tank, after gaining the heating energy in the collector. Then, it enters the pump after the heat transferring and passing the second storage tank and then reaches the pump inlet. It is necessary to mention that the second tank is located at higher altitude than the pump, in order to produce the static pressure for prevention of cavitation in

the pump inlet. After the pump, the working fluid reaches the collector through flowmeter. The flowmeter with uncertainty of ± 2% was used to measure the volume flow rate. Some valves are installed for better controlling of the fluid flow. Transparent temperature-resistant PVC tubes are used for connecting the equipment together. The pump is a Grundfos-UPS 25-60 series which has the capability to work with warm fluid in three different speeds and with a maximum flow rate of 4.3 $m^3\ h^{-1}$. To measure the flow rate, a rotameter which has the maximum flow capacity of 1000 $l\ h^{-1}$ has been used. The Rosemount pressure transmitter model CD2 with the accuracy of 0.001 mbar was utilized for measuring the occurred pressure drop in the collector. The inlet and outlet temperatures of the collector were measured by two RTD-type PT 100 thermocouples with 0.1 °C accuracy. These thermocouples were installed in the nearest position to the inlet and outlet headers. The absorber plate temperature was measured by four numbers of K-type thermocouples with 0.1 °C accuracy. Also, the environmental temperature was determined by a portable thermocouple. The heat flux of the solar radiation is measured by a TES-1333R solar power meter. Prova AVM-305 model anemometer was used to measure the speed of the wind. Furthermore, a heat exchanger is utilized in cycle to maintain the inlet temperature of working fluid according to ASHRAE Standard. The error of instrument devices is given in Table 1, and the specifications of collector are given in Table 2. It should be noted that all apparatus has been calibrated in one of the calibrator companies in Tehran, Iran.

Table 1 The error of instrument devices

Instruments	Error
Flowmeter	± 2%
Thermometer (TES-1317R)	1.5%
Anemometer (Prova AVM-305)	± 3%, ± 0.2 m s^{-1}
Solar power meter (TES-1333R)	± 2.5%

Table 2 The specification of flat-plate collector

Specification	Dimension
Collector occupied volume/cm^3	112 × 52 × 20
Riser number	4
Riser diameter/mm	10
Riser length/m	0.9
Header diameter/mm	22
Absorber width/m	0.65
Absorber length/m	1.5

Table 3 Operating conditions for the chrome plating process

Temperature/°C	35
PH	4<
Anode	Lead
Cathodic current density/A dm^{-2}	35

Coating deposition

The black chrome, carbon, and matt black paint were chosen owing to good optical properties and good thermal conductivity [33]. The impurities were removed by washing the plates with distilled water. To prepare the chrome plating bath, chrome sulfate, cobalt chloride, sodium hypophosphite, and sodium phosphate dihydrogen were mixed together, and then, distilled water was added to them. The positive ions were deposited on the copper plate by applying an electric current. Table 3 presents the optimal conditions for the chrome plating process.

The matt black paint was coated by spraying. The carbon film was deposited on the copper plate under vacuum sintering conditions. Carbon coating was deposited on the plate in a vacuum chamber. The chamber was evacuated by argon injection. The vacuum condition was maintained at a pressure of 150 Pa using a vacuum pump. The sample was applied at a voltage of 1.5 volts.

The optical absorptivity of the black paint, the black chrome coating, and the carbon coating is measured, which is approximately 0.85, 0.93, and 0.95, respectively. The absorptance and reflectance coefficients were measured by the Avaspec machine, manufactured by the Spanish Avantes Company, with an accuracy of 0.08 nm [33].

Figures 2, 3, and 4 display the FESEM analysis images for three types of coating on the copper plate. As can be seen, the black paint coating has a smooth surface compared to the carbon coating. The radiative characteristics of optically smooth bodies can be prognosticated within the limitations of electromagnetic theory. When the surface optical roughness is larger than about 1, there are various reflections in the cavities among roughness elements. This enhances the trapping of disturbance radiation, thereby improving the observed surface absorptivity and consequently its emissivity. When roughness is high, it has a significant impact on directional emission and reflection. When the optical roughness is small (< 1), the effects of various reflections in roughness holes are regularly small, and the hemispherical properties come near to those for optically smooth surfaces. As a result of diffraction impacts, the directional features can be remarkably affected by the roughness. Therefore, the carbon coating has high absorption owing to trapping the light and avoiding the reflection of the light. The higher porosity leads to trapping more light [33].

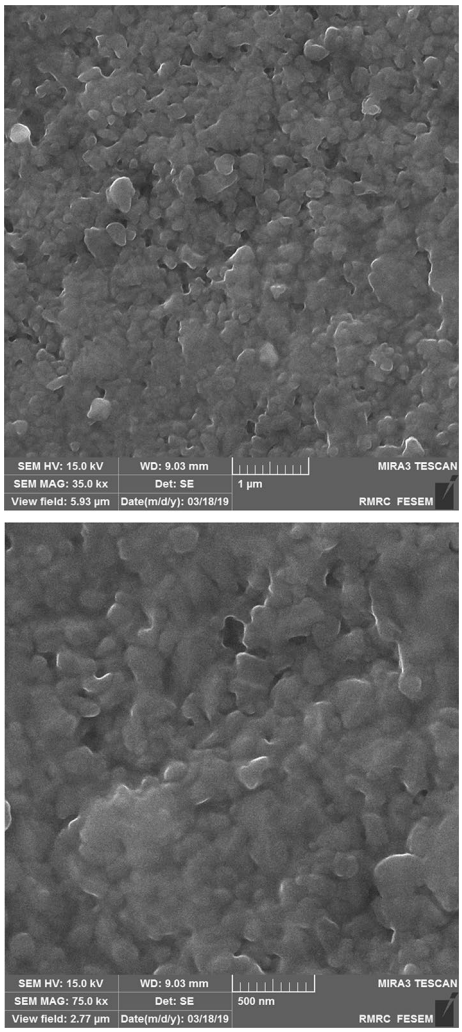

Fig. 2 FESEM images of black paint coating on copper plate in two zoom modes

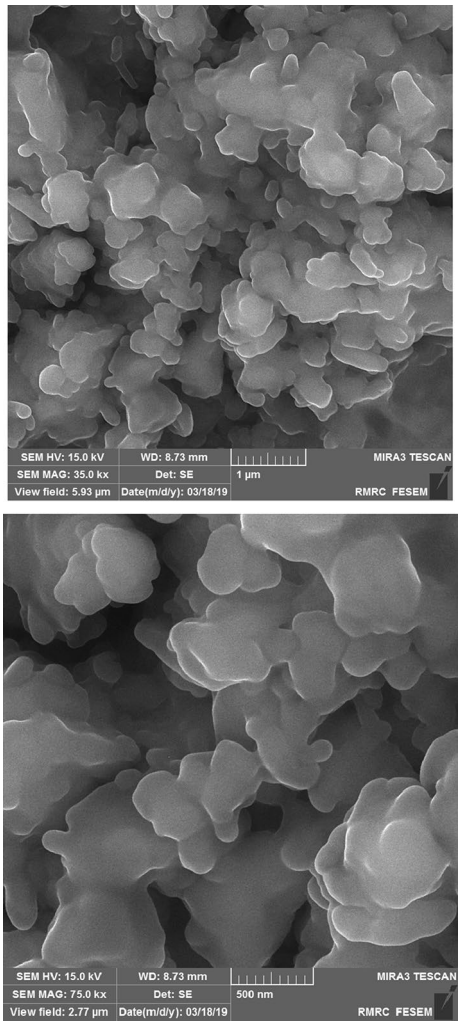

Fig. 3 FESEM images of black chrome coating on copper plate in two zoom modes

Testing methodology

The ASHRAE 93:2010 standard can be used to investigate the thermal performance of flat-plate collectors under steady state conditions. To determine the thermal efficiency of the collector in outdoors, there are some limitations. The wind velocity must be between 2 and 4 m s^{-1}. The minimum solar radiation on a plate perpendicular to direct radiation shall not be less than 800 W m^{-2}. The tests must be performed at a time when the sky is smooth, so that the maximum variation of solar irradiance is not greater than 32 W m^{-2} at a time interval of 10 min or twice the time constant, whichever is the greater, before and during data recording. The ambient temperature range must be less than 30 °C. The inlet temperature of working fluid must be constant, and the maximum deviation from ambient temperature is ± 1°C.

Time constant

Determining the response time of the solar collector is essential to evaluate the collector's transient performance and to select the correct time interval to test a stable state or Gaussian state. The time constant parameter is given by [34]:

$$(T_{f,o}(\tau) - T_{f,i})/(T_{f,o,initial} - T_{f,i}) = 0.632 \quad (1)$$

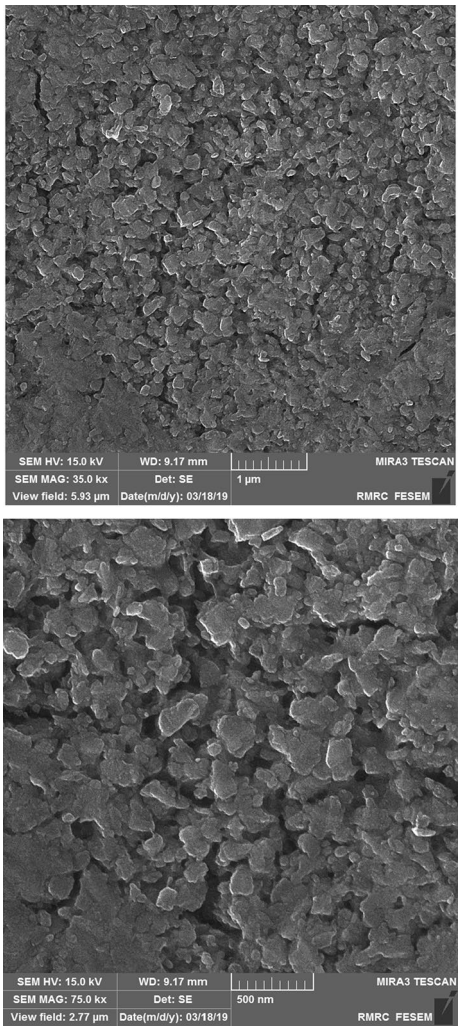

Fig. 4 FESEM images of carbon coating on copper plate in two zoom modes

Thermal performance analysis

The useful energy gain, $\dot{Q}_u$, can be obtained by measuring the inlet and outlet temperatures of working fluid:

$$\dot{Q}_u = \dot{m}C_p(T_{f,o} - T_{f,i}) \tag{2}$$

Furthermore, the useful energy gained by collector can be expressed in terms of the absorbed energy and the lost energy from the absorber plate:

$$\dot{Q}_u = A_c F_R\left[G(\tau\alpha)_e - U_L(T_{f,i} - T_a)\right] \tag{3}$$

where A_c is the area of absorber plate, $T_{f,i}$, $T_{f,o}$, and T_a are the fluid inlet temperature, fluid outlet temperature, and ambient temperature, respectively. In addition, F_R is the heat removal factor, G is the solar radiation on the collector, $(\tau\alpha)_e$ is the effective coefficient of transmission–absorption, and U_L is the heat loss coefficient.

The thermal efficiency can be calculated from Eq. (4):

$$\eta = \dot{Q}_u/GA_c = \dot{m}C_p(T_{f,o} - T_{f,i})/GA_c \tag{4}$$

Furthermore, the thermal efficiency can be obtained by substituting Eq. (3) for Eq. (4):

$$\eta = F_R(\tau\alpha)_e - (F_R U_L \times (T_{f,i} - T_a)/G) \tag{5}$$

When the curve of the thermal efficiency variation versus $(T_{f,i} - T_a)/G$ is plotted, the intercept and slope of linear curve show optical efficiency $F_R(\tau\alpha)_e$ and removed energy parameter $F_R U_L$ (Fig. 4).

Uncertainty analysis

Uncertainty values provide the accuracy and reliability of the test results. Therefore, uncertainty determines the quality of the test and the results. The uncertainty of the results can be estimated using a root-sum-square combination of the effects of each input by Kline and McClintock formula [36]:

$$\delta R = \left\{\left(\sum_{i=1}^{N}(\partial R/\partial X_i)\cdot\delta X_i\right)^2\right\}^{1/2} \tag{6}$$

where $\frac{\partial R}{\partial X_j}$ shows the sensitivity coefficient for the result R toward X_j. The uncertainty of the thermal efficiency of the FPC can be given by Eq. (7):

$$\frac{\delta\eta}{\eta} = \left[(\delta\dot{m}/\dot{m})^2 + (\delta C_p/C_p)^2 + (\delta(T_o - T_{in})/(T_o - T_{in}))^2 + (\delta G/G)^2 + (\delta A/A)^2\right]^{0.5} \tag{7}$$

$\delta\dot{m}/\dot{m} \le 0.015$, $\delta(T_o - T_{in})/(T_o - T_{in}) \le 0.015$, $\delta G/G \le 0.025$, $\delta\eta/\eta \le 3.28\%$.

By ignoring the variation of C_p and A_c, the maximum uncertainty of thermal efficiency is approximately 3.28%.

Results and discussion

The evaluation of time constant is one of the important parameters (Eq. 1) showing the time needed to achieve a stable system. Figure 5 presents the variation of time constant with the Reynolds number in the range of 247–743 in which the collector with the carbon-coated absorber plate

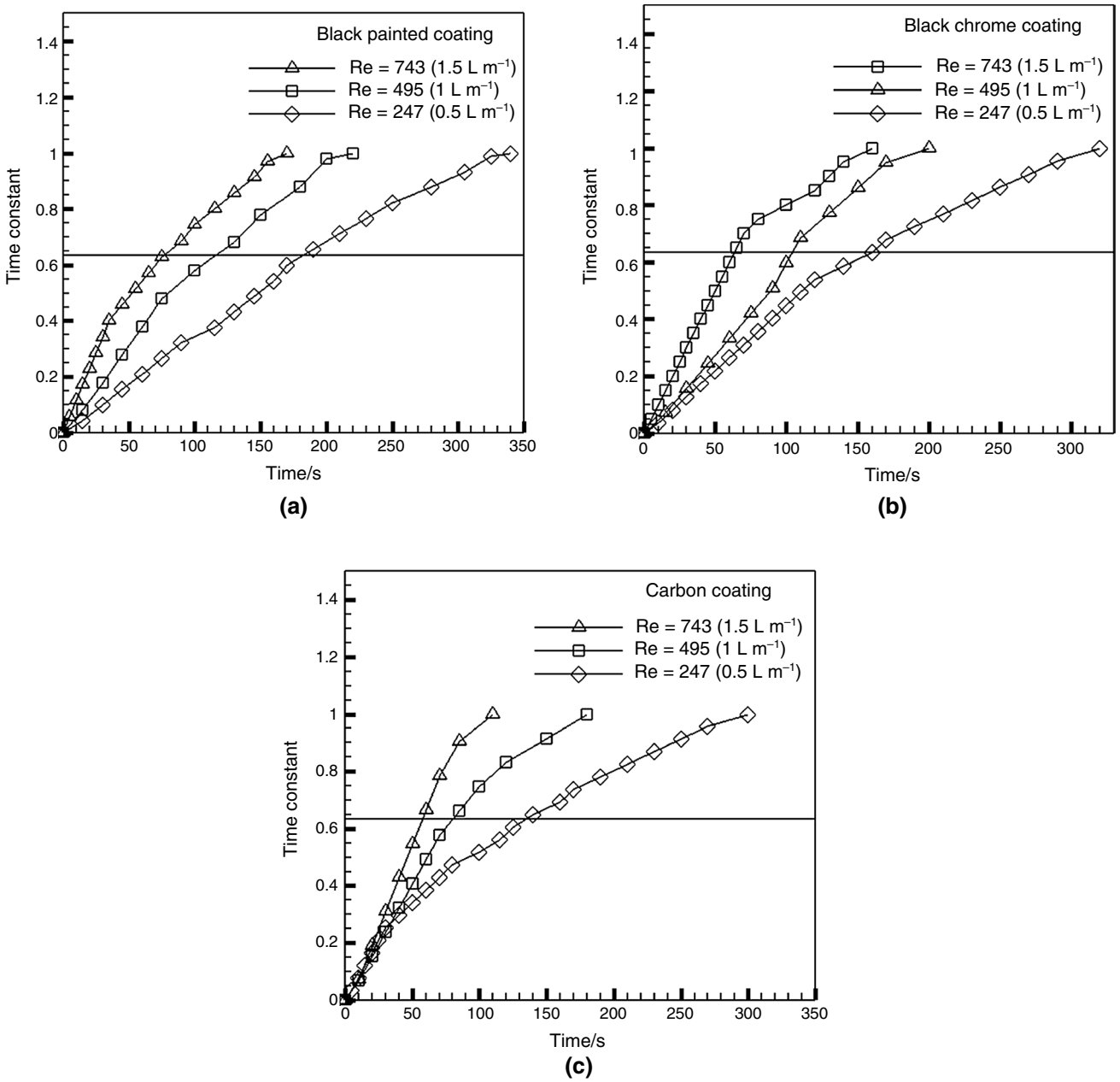

Fig. 5 The comparison of the time constant for the collector with different coated absorber plates: **a** black-painted coating, **b** black chrome coating, and **c** carbon coating

has the quickest response time owing to lower heat loss. The time constants of the collector with the black paint, the black chrome-coated, and the carbon-coated absorber plates for Reynolds number of 743 are approximately 180 s, 160 s, and 140 s, respectively.

The operating conditions during the test are in accordance with ASHRAE Standard 93 (2010). Figure 6 shows the measured data to calculate the thermal efficiency of the collector. The measured data have been recorded between 10 o'clock and 13:30 in May 20, 2019, to May 26, 2019.

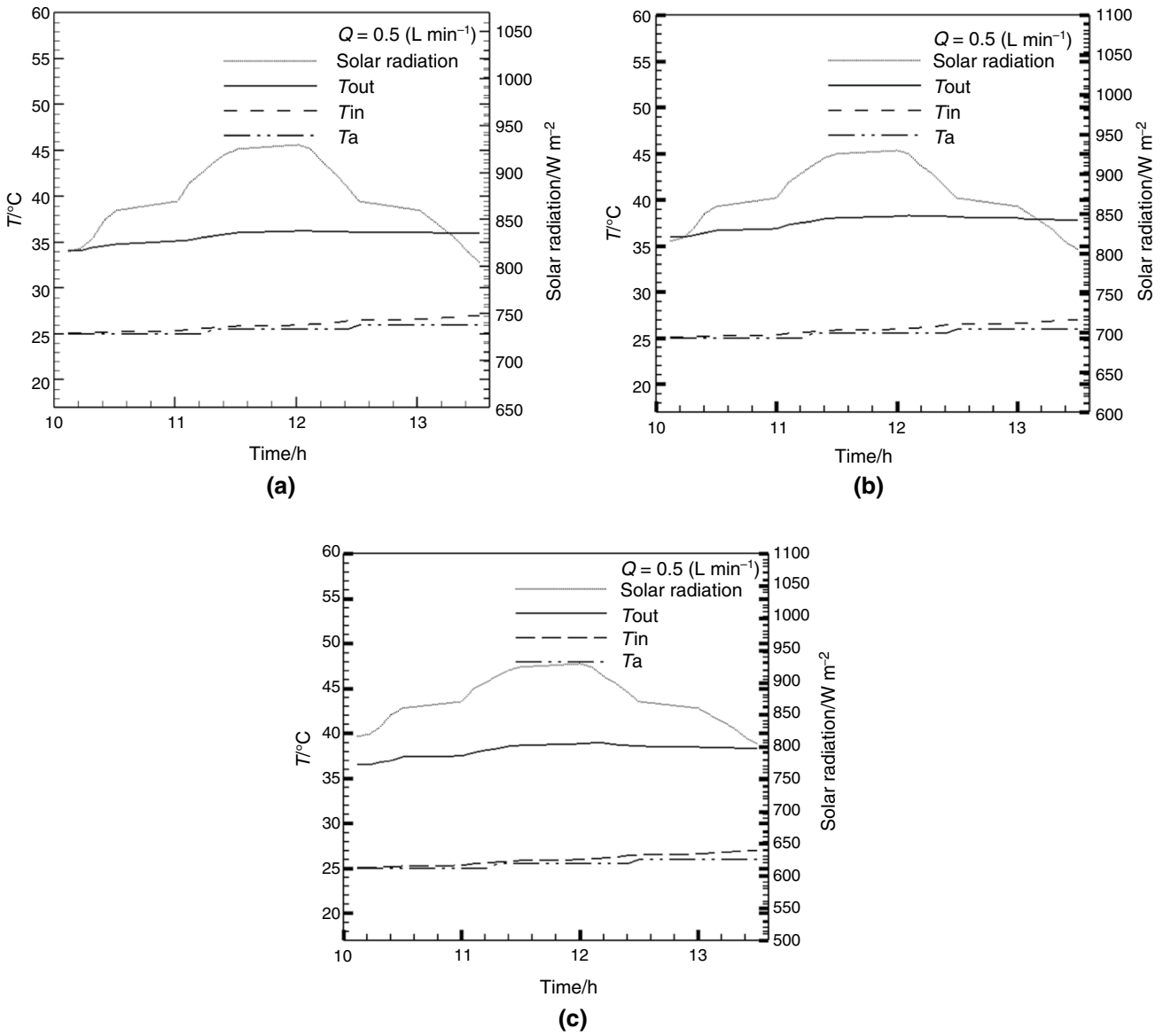

Fig. 6 Measured data during the test for **a** the black paint coated absorber plate, **b** the chrome-coated absorber plate, and **c** the carbon-coated absorber plate

The reason for choosing this interval time is because of the limitations specified for the solar noon parameter in the ASHRAE Standard. The thermal efficiency data were collected symmetrically with respect to solar noon according to the ASHRAE Standard. It can be seen that the amount of solar radiation increased step by step with the start of the test, and in the final hours of the test, this amount decreased with the same behavior. It should be noted that the maximum amount of this quantity occurs around 12 o'clock. By investigating the outlet temperature data, it is found that the outlet temperature of the collector with a carbon-coated absorber plate is higher than the collector with black chrome-coated

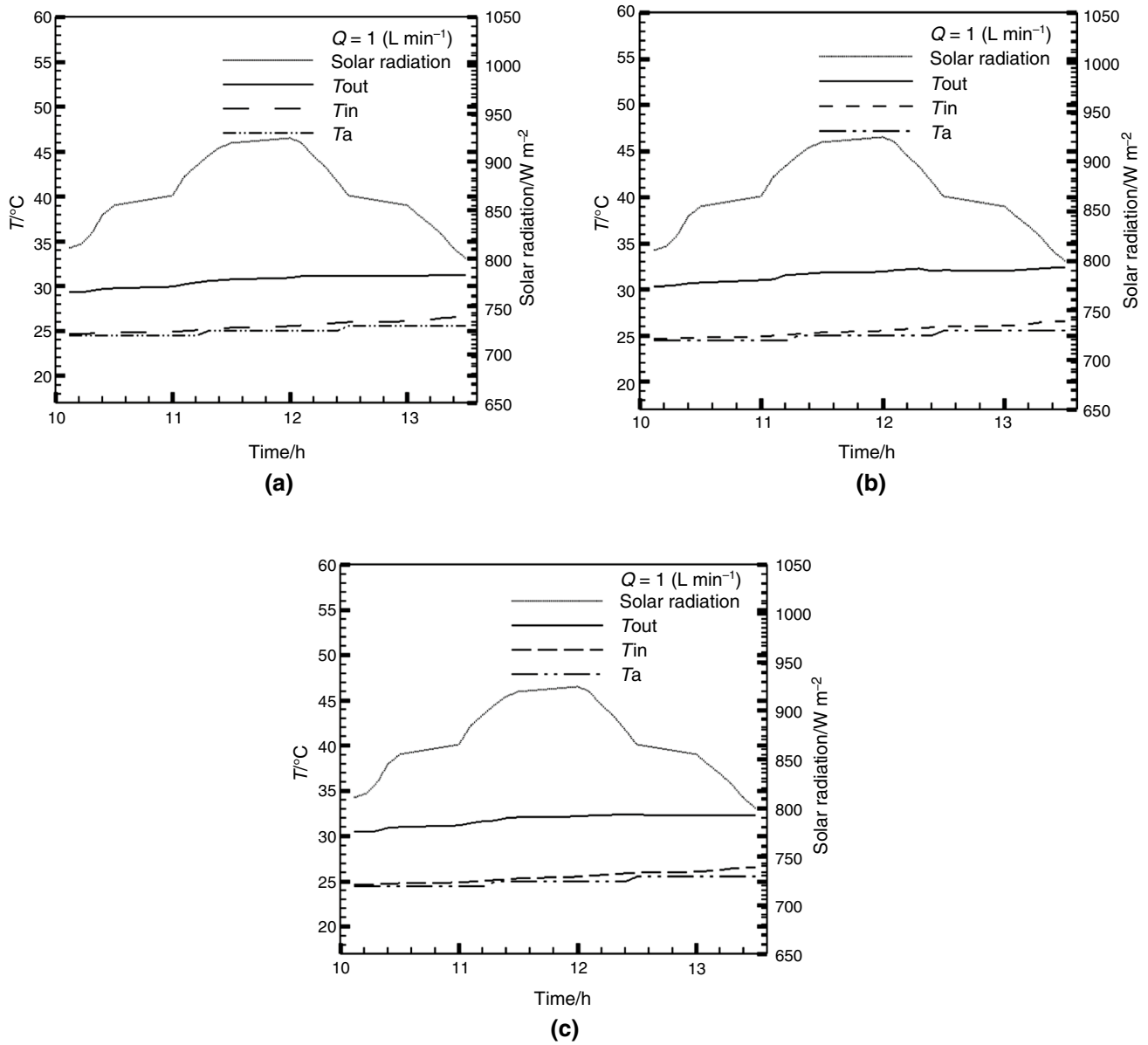

Fig. 6 (continued)

absorber plate and the collector with black-painted absorber plate. For three types of coatings, the maximum outlet temperature in all of the investigated flow rates is observed in 0.5 L min^{-1}, which is approximately 39 °C for black carbon coating, 37 °C for black chrome coating, and 33° C for black painted. The ambient temperature slightly increases during the testing process. According to ASHRAE Standard, the inlet temperature shall be always ± 1 degree of the ambient temperature. So the same trend for inlet temperature can be seen.

Figure 7 presents the variation of the thermal efficiency with the volume flow rates. As can be observed, the

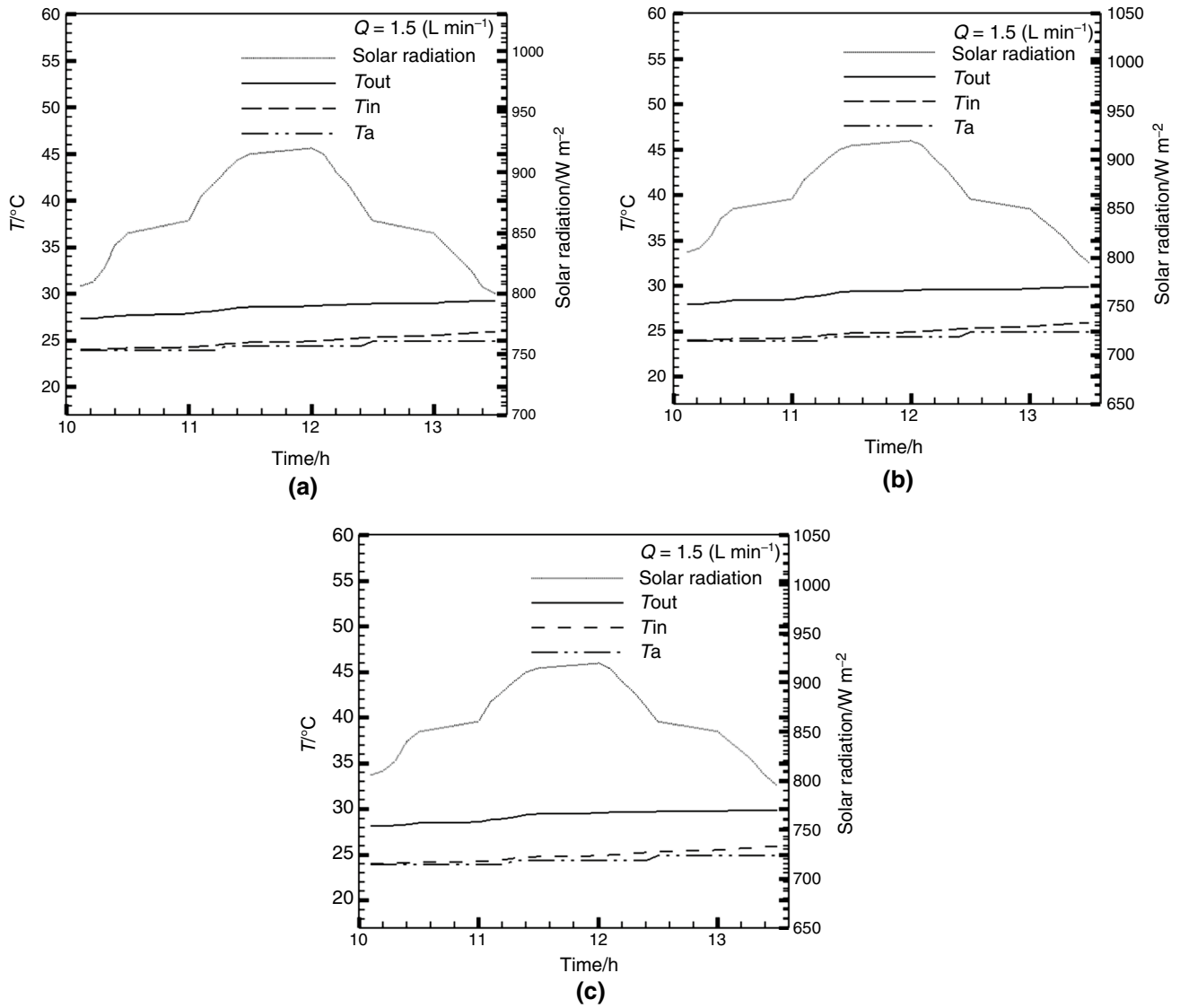

Fig. 6 (continued)

Reynolds number significantly affects the absorbed and removed energy parameter. It causes increasing absorption and decreasing removed energy parameter, leading to improvement on the thermal efficiency. The high emissivity of black paint leads to higher heat loss and lower thermal performance. The thermal efficiency of the carbon-coated absorber plate and the black chrome absorber plate is approximately 13% and 11.3% higher than that of the collector with the black-painted coating on absorber plate. The thermal efficiency of the carbon coating and the black chrome is higher than the black paint, since they have higher optical absorptance. Therefore, lower emissivity and higher absorptivity of the carbon coating and the black chrome in comparison with black paint result in higher thermal performance. As Fig. 7 shows, the line slope and the coordinate distance of the collector with the carbon-coated absorber plate are equal to 7.264 and 0.7025, respectively, which are equal to $\frac{F_R U_L}{G}$ and $F_R(\tau\alpha)_e$. As can be seen from the figure, the thermal efficiency trend decreases for all flow rates, which have been reported in [24, 37].

As Fig. 8 shows, in a collector's thermal efficiency variation in the black-painted absorber plate, the black

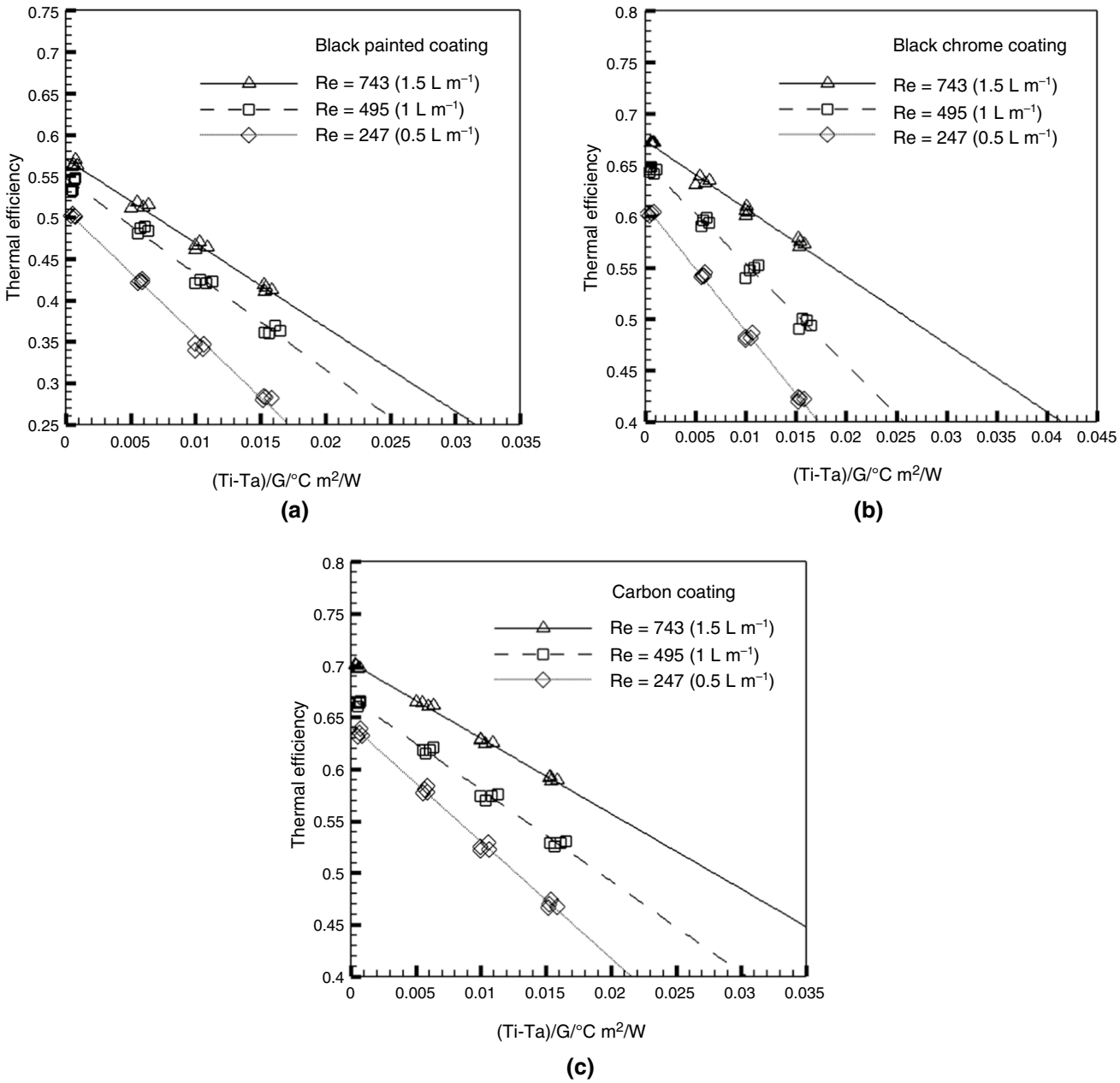

Fig. 7 The efficiency of the solar collector with different coated absorber plates: **a** black-painted coating, **b** black chrome coating, and **c** carbon coating

chrome-coated absorber plate, and the carbon-coated absorber plate versus the Reynolds number, the absorbed energy parameter enhances with increasing the Reynolds number. The collector with the carbon-coated absorber plate has the highest thermal efficiency approximately to 63.4%, 66.3%, and 69.4% at the Reynolds number of 247, 495, and 743, respectively. Furthermore, the removed energy parameter in the collector with the carbon-coated absorber plate decreases by approximately 15%, 19%, and 35.4%, compared to the collector with the black chrome-coated absorber plate, in which it decreases by 23.4%, 25.04%, and 28.4% at the Reynolds number of 247, 495, and 743, respectively. The FESEM analysis images for three types of coatings on the copper plate indicate that the black paint coating has a smooth surface compared to the carbon coating. Thus, the carbon coating has high absorption owing to trapping the light and avoiding the reflection of the light.

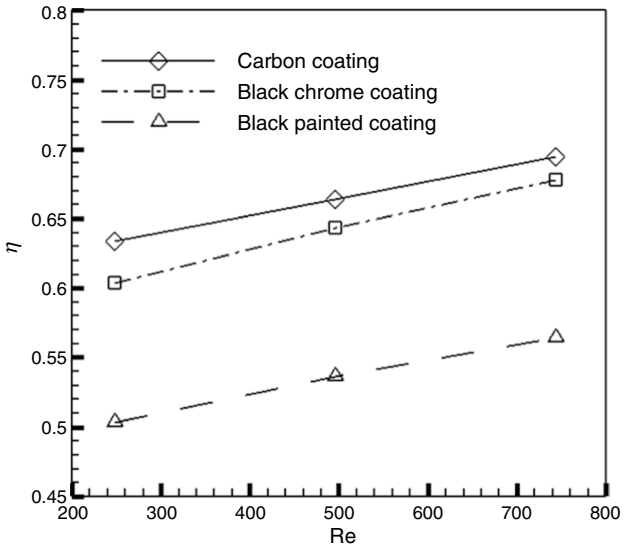

Fig. 8 Variations of the thermal efficiency with the Reynolds number

Table 4 Costs of collector manufacturing

Cases	Matt black paint	Black chrome	Carbon
Setup manufacturing cost (USD)	1729.25	1729.25	1729.25
Coating cost (USD)	12.17	14.84	16.3
Thermal efficiency	56.4%	67.7%	69.4%

Investment costs

From a general view, cost savings can be divided into two groups of impact: direct and indirect. The concept of direct impact includes costs that are directly related to the collector assembly such as the procurement of raw materials, manufacturing, etc., while the indirect impact is not relevant to the collector owner, but spread among the collector installer, the service, or the federal and state government. These destructive costs show the influence of the pollutants from the collector manufacturing, but the economic or environmental consequences of coating are not involved. In Table 4, all costs of collector manufacturing and coating of absorber plate are presented. As can be seen, the costs of carbon and black chrome coatings are USD 4.13 and USD 2.67 higher than matt black paint coating, respectively, but the thermal efficiency of the collector with carbon-coated absorber plate and the collector with black chrome-coated absorber plate is higher than the collector with matt black-painted absorber plate. The key question is whether the increase in thermal efficiency against the increased cost of coating is cost-effective or not. In order to closely scrutinize the issue, the black coated collector is considered as the base of our calculations due to its lower efficiency. According to the calculations considering the reduction of the absorber plate area, the cost for the carbon-coated case is USD 5.31 and USD 4.51 less than the matt black-painted case, respectively. The reason is the thermal efficiency increasing and, consequently, the reduction of the absorber plate area and its mass which will save the cost of providing the adsorbent coating and coating. It should be noted that considering cost saving in assembly manufacturing by glazing area reduction, riser length decrease, and so on alongside the indirect cost saving, the use of selective coating will be more preferable.

Conclusions

An experimental study into the thermal efficiency of three flat-plate collectors with the black-painted absorber plate, the black chrome-coated absorber plate, and the carbon-coated absorber plate was conducted according to ASHRAE Standard. The flat-plate collector with the carbon-coated absorber plate had the highest thermal efficiency owing to higher optical absorptivity. The thermal efficiency increases by approximately 13% and 11.3% for the flat-plate collector with the carbon-coated absorber plate and the black chrome-coated absorber plate compared to the collector with the black-painted absorber plate. Furthermore, the energy removed parameter decreases by approximately 28.4% and 35.4% for the collector with the carbon-coated absorber plate and the black chrome-coated absorber plate, respectively. The use of selective coatings enhances the thermal efficiency and decreases the heat loss owing to higher optical absorptivity and lower emissivity.

The results demonstrate that the use of the black chrome and the carbon coatings on absorber plates of FPCs is potential owing to its high capacity to increase the thermal efficiency of the collectors.

References

1. Duffie JA, Beckman, WA, Solar engineering of thermal processes, New York: Wiley; 2013. https://www.wiley.com/en-us/Solar+Engineering+of+Thermal+Processes,+4th+Edition-p-9780470873663. Accessed 17 Apr 2019.
2. Sakhaei SA, Valipour MS. Performance enhancement analysis of the flat plate collectors: a comprehensive review. Renew Sustain Energy Rev. 2019;102:186–204. https://doi.org/10.1016/J.RSER.2018.11.014.
3. Asadi J, Amani P, Amani M, Kasaeian A, Bahiraei M. Thermo-economic analysis and multi-objective optimization of absorption cooling system driven by various solar collectors. Energy Convers Manag. 2018;173:715–27. https://doi.org/10.1016/j.enconman.2018.08.013.

4. Nazari S, Safarzadeh H, Bahiraei M, Experimental and analytical investigations of productivity, energy and exergy efficiency of a single slope solar still enhanced with thermoelectric channel and nanofluid. Renew Energy 2019;729–744. https://doi.org/10.1016/j.renene.2018.12.059.
5. Jaisankar S, Radhakrishnan TK, Sheeba KN, Suresh S. Experimental investigation of heat transfer and friction factor characteristics of thermosyphon solar water heater system fitted with spacer at the trailing edge of left-right twisted tapes. Energy Convers Manag. 2009;50:2638–49. https://doi.org/10.1016/J.ENCONMAN.2009.06.019.
6. Ananth J, Jaisankar S. Experimental studies on heat transfer and friction factor characteristics of thermosyphon solar water heating system fitted with regularly spaced twisted tape with rod and spacer. Energy Convers Manag. 2013;73:207–13. https://doi.org/10.1016/J.ENCONMAN.2013.04.022.
7. García A, Martin RH, Pérez-García J. Experimental study of heat transfer enhancement in a flat-plate solar water collector with wire-coil inserts. Appl Therm Eng. 2013;61:461–8. https://doi.org/10.1016/J.APPLTHERMALENG.2013.07.048.
8. Ananth J, Jaisankar S. Investigation on heat transfer and friction factor characteristics of thermosiphon solar water heating system with left-right twist regularly spaced with rod and spacer. Energy. 2014;65:357–63. https://doi.org/10.1016/J.ENERGY.2013.12.001.
9. Jouybari HJ, Saedodin S, Zamzamian A, Nimvari ME, Wongwises S. Effects of porous material and nanoparticles on the thermal performance of a flat plate solar collector: an experimental study. Renew Energy. 2017;114:1407–18. https://doi.org/10.1016/J.RENENE.2017.07.008.
10. Javaniyan Jouybari H, Saedodin S, Zamzamian A, Nimvari ME. Experimental investigation of thermal performance and entropy generation of a flat-plate solar collector filled with porous media. Appl Therm Eng. 2017;127:1506–17. https://doi.org/10.1016/j.applthermaleng.2017.08.170.
11. Chen Z, Gu M, Peng D. Heat transfer performance analysis of a solar flat-plate collector with an integrated metal foam porous structure filled with paraffin. Appl Therm Eng. 2010;30:1967–73. https://doi.org/10.1016/J.APPLTHERMALENG.2010.04.031.
12. Bazri S, Badruddin IA, Naghavi MS, Bahiraei M. A review of numerical studies on solar collectors integrated with latent heat storage systems employing fins or nanoparticles. Renew Energy. 2018;118:761–78. https://doi.org/10.1016/j.renene.2017.11.030.
13. Nazari S, Safarzadeh H, Bahiraei M. Performance improvement of a single slope solar still by employing thermoelectric cooling channel and copper oxide nanofluid: an experimental study. J Clean Prod. 2019;208:1041–52. https://doi.org/10.1016/j.jclepro.2018.10.194.
14. Olia H, Torabi M, Bahiraei M, Ahmadi MH, Goodarzi M, Safaei MR. Application of nanofluids in thermal performance enhancement of parabolic trough solar collector: state-of-the-art. Appl. Sci. 2019;9:463. https://doi.org/10.3390/app9030463.
15. Kasaeian A, Eshghi AT, Sameti M. A review on the applications of nanofluids in solar energy systems. Renew Sustain Energy Rev. 2015;43:584–98. https://doi.org/10.1016/j.rser.2014.11.020.
16. Tayebi R, Akbarzadeh S, Valipour MS. Numerical investigation of efficiency enhancement in a direct absorption parabolic trough collector occupied by a porous medium and saturated by a nanofluid. Environ Prog Sustain Energy. 2018. https://doi.org/10.1002/ep.13010.
17. Said Z, Sabiha MA, Saidur R, Hepbasli A, Rahim NA, Mekhilef S, Ward TA. Performance enhancement of a flat plate solar collector using titanium dioxide nanofluid and Polyethylene Glycol dispersant. J Clean Prod. 2015;92:343–53. https://doi.org/10.1016/J.JCLEPRO.2015.01.007.
18. Noghrehabadi A, Hajidavalloo E, Moravej M. An experimental investigation of a 3-D solar conical collector performance at different flow rates. J Heat Mass Transf Res. 2016;1:57–66.
19. Bellos E, Tzivanidis C, Tsimpoukis D. Enhancing the performance of parabolic trough collectors using nano fluids and turbulators. Renew Sustain Energy Rev. 2018;91:358–75. https://doi.org/10.1016/j.rser.2018.03.091.
20. Frank G, Kauer E, Köstlin H, Schmitte FJ. Transparent heat-reflecting coatings for solar applications based on highly doped tin oxide and indium oxide. Sol Energy Mater. 1983;8:387–98. https://doi.org/10.1016/0165-1633(83)90004-7.
21. Amrutkar SK, Solar Flat Plate Collector Analysis, IOSR J Eng. 2012;2:207–213.
22. Föste S, Ehrmann N, Giovannetti F, Rockendorf G. Basics for the development of a high efficiency flat-plate collector with a selectively coated double glazing, 30th ISES Bienn. Sol World Congr. 2011;3:2469–74. https://doi.org/10.18086/swc.2011.19.14.
23. Akbarzadeh S, Valipour MS. Heat transfer enhancement in parabolic trough collectors: A comprehensive review. Renew Sustain Energy Rev. 2018;92:198–218. https://doi.org/10.1016/J.RSER.2018.04.093.
24. Bhide VG, Vaishya JS, Nagar VK, Sharma SK. Choice of selective coating for flat plate collectors. Sol Energy. 1982;29:463–5. https://doi.org/10.1016/0038-092X(82)90054-8.
25. Dias D, Rebouta L, Costa P, Al-Rjoub A, Benelmeki M, Tavares CJ, Barradas NP, Alves E, Santilli P, Pischow K. Optical and structural analysis of solar selective absorbing coatings based on $AlSiO_x$:W cermets. Sol Energy. 2017;150:335–44. https://doi.org/10.1016/j.solener.2017.04.055.
26. Ning Y, Wang W, Wang L, Sun Y, Song P, Man H, Zhang Y, Dai B, Zhang J, Wang C, Zhang Y, Zhao S, Tomasella E, Bousquet A, Cellier J. Optical simulation and preparation of novel Mo/ZrSiN/ZrSiON/SiO_2 solar selective absorbing coating. Sol Energy Mater Sol Cells. 2017;167:178–183. https://doi.org/10.1016/j.solmat.2017.04.017.
27. Yin Y, Pan Y, Hang LX, McKenzie DR, Bilek MMM. Direct current reactive sputtering Cr–Cr_2O_3 cermet solar selective surfaces for solar hot water applications, Thin Solid Films. 2009:517:1601–6. https://doi.org/10.1016/J.TSF.2008.09.082.
28. Voinea M, Bogatu C, Chitanu GC, Duta A. Copper cermets used as selective coatings for flat plate solar collectors. Rev Chim. 2008;59:1–6.
29. Konttinen P, Lund PD. Microstructural optimization and extended durability studies of low-cost rough graphite–aluminium solar absorber surfaces. Renew Energy. 2004;29:823–39. https://doi.org/10.1016/J.RENENE.2003.11.008.
30. Moncada MLT, Muñoz BC, Yoshida MM, Rodríguez RD. Comparative experimental study of new absorbent surface coatings for flat plate solar collectors, Energy Procedia. 2014;57:2131–8. https://doi.org/10.1016/j.egypro.2014.10.179.
31. Shamshirgaran SR, Khalaji Assadi M, Badescu V, Al-Kayiem HH. Upper limits for the work extraction by nanofluid-filled selective flat-plate solar collectors. Energy. 2018;160:875–85. https://doi.org/10.1016/J.ENERGY.2018.06.154.
32. Alami AH, Aokal K. Enhancement of spectral absorption of solar thermal collectors by bulk graphene addition via high-pressure graphite blasting. Energy Convers Manag. 2018;156:757–64. https://doi.org/10.1016/J.ENCONMAN.2017.11.040.
33. Kasaeian A, Daviran S, Azarian RD. Optical and thermal investigation of selective coatings for solar absorber tube. Int J Renew Energy Res. 2016;6:15–20.
34. Kasaeian A, Daviran S, Azarian RD, Rashidi A. Performance evaluation and nanofluid using capability study of a solar parabolic trough collector. Energy Convers Manag. 2015;89:368–75. https://doi.org/10.1016/j.enconman.2014.09.056.

35. Standards A, November C, Board A, Janu D. Methods of testing to determine the thermal performance of solar collectors, 1991;1986.
36. Moffat RJ. Describing the uncertainties in experimental results. Exp Therm Fluid Sci. 1988;1:3–17. https://doi.org/10.1016/0894-1777(88)90043-X.
37. Müller S, Giovannetti F, Reineke-Koch R, Kastner O, Hafner B. Simulation study on the efficiency of thermochromic absorber coatings for solar thermal flat-plate collectors. Solar Energy. 2019;188:865–74.